J. Fluid Mech. (1971), *vol.* 47, *part* 1, *pp.* 93–112
Printed in Great Britain

Comparison of theory and experiment in peristaltic transport

By F. C. P. YIN AND Y. C. FUNG

Department of Aerospace and Mechanical Engineering Sciences
University of California, San Diego, La Jolla, California

(Received 23 March 1970)

Various theoretical aspects of peristaltic motion have attracted considerable attention in the recent literature. There also exists a difference of opinion concerning the definition of peristaltic reflux. Thus far, there has been no completely satisfactory experimental verification of any of the theoretical analyses. The present article describes some details of an experimental work which was carried out to verify the theoretical analysis of peristaltic transport in a two-dimensional channel with one fixed wall and one flexible wall on which a travelling sine wave is imposed. An approximate correction for finite width was introduced. Comparison of the theoretical and experimental results shows a good agreement and gives verification to the theoretical analysis. In the light of the experimental results, a discussion of the different definitions of peristaltic reflux is presented.

1. Introduction

Recently, various theoretical aspects of peristaltic transport have attracted considerable attention (see Barton & Raynor 1968; Burns & Parks 1967; Fung & Yih 1968; Hanin 1968; Shapiro 1967; Shapiro, Jaffrin & Weinberg 1969; Yin & Fung 1969; Yin 1970; Zien & Ostrach 1970). It is desirable to verify the theoretical analyses with experimental work. For practical reasons, the simplest experimental set-up utilizes a rectangular cross-section channel with three fixed walls and one flexible wall on which the travelling wave is imposed. Latham (1966) performed a number of experiments using a similar geometry which was obtained by flattening a round plastic tube. He compared the experimental results with the results obtained from the two-dimensional, long wavelength, zero Reynolds number theory of Shapiro (1967). Besides completely ignoring the effects of the side walls of the tube, Latham made a direct comparison between the experiment, which had only one waving wall, and the theory in which travelling waves were imposed on both walls of a two-dimensional channel. Therefore, his comparison between theory and experiment was not entirely satisfactory.

The purpose of the present article is to offer a more detailed comparison between theory and experiment for small amplitude peristaltic motion at finite Reynolds number and finite wavelength.

In order to employ a theoretical model which more closely matched the

experimental apparatus, the theoretical analysis of Fung & Yih (1968) was extended and modified to apply to the case of a two-dimensional channel with one fixed wall and one flexible wall. An approximate method was then introduced to correct for the three-dimensional effects due to finite width-to-height ratio. The correct theoretical results are compared with the experimental results.

In addition to studying the time-averaged flow quantities, details of the fluid motion were studied by examination of the particle trajectories. Some details of the theoretical analysis are presented in § 2. Details of the experimental work undertaken to verify the analysis are presented in § 3. Results and conclusions are discussed in § 4.

2. Theoretical analysis

The analysis was made for the case of a two-dimensional channel with one fixed wall and one flexible wall on which a travelling sine wave is imposed (see figure 1). This work is an extension and modification of the corresponding analysis for the

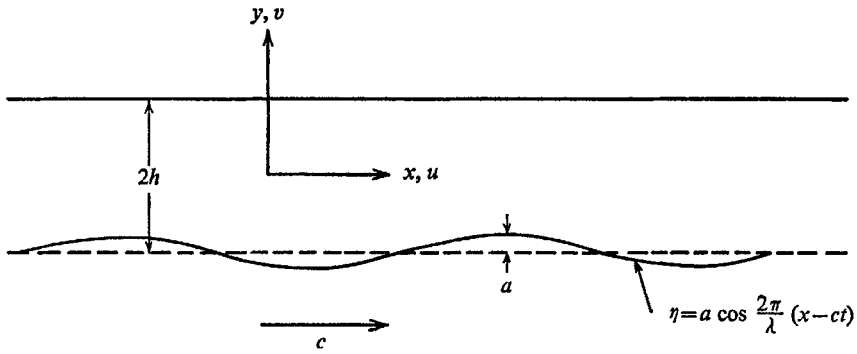

FIGURE 1. Geometry of two-dimensional channel and travelling wave system.

case of a two-dimensional channel for which travelling sine waves were imposed on both walls (Fung & Yih 1968). In the present analysis, in addition to the time-averaged velocity and flow rate expressions, explicit expressions for the axial and transverse velocity components are obtained. A numerical integration of the velocity component expressions yields the particle trajectories.

The basic assumptions used herein are the same as in the previous analysis. A small amplitude travelling sine wave is assumed to be imposed on the flexible wall of a two-dimensional channel. The fluid contained within the channel is assumed to be Newtonian viscous, homogeneous, and incompressible. The fluid is assumed to satisfy the non-slip conditions at the boundary with the walls. The waving wall is assumed to have only transverse displacements without any lateral displacement. In order to clearly demonstrate the effect of the peristaltic motion itself, the analysis is carried out for the special case of a zero mean imposed pressure gradient.

Since the methods of solution and the notations are identical to those used in the previous analysis (Fung & Yih 1968), only the most important equations will be presented herein. Details can be found in the dissertation by Yin (1970).

The governing equation of motion in non-dimensional form is

$$\frac{\partial}{\partial t}\nabla^2\psi+\frac{\partial\psi}{\partial y}\nabla^2\left(\frac{\partial\psi}{\partial x}\right)-\frac{\partial\psi}{\partial x}\nabla^2\left(\frac{\partial\psi}{\partial y}\right)=\frac{1}{R_e}\nabla^2\nabla^2\psi, \tag{1}$$

where $R_e = ch/\nu$ is the Reynolds number based on channel mean half-height h, wave speed c, and kinematic viscosity ν. ψ is the two-dimensional stream function and ∇^2 is the two-dimensional Laplacian operator. The wavy channel is illustrated in figure 1 in which physical variables are shown. In subsequent equations and figures non-dimensional variables are used. The normalization is based on h and c, so that

$$\tilde{x} = x/h, \quad \tilde{y} = y/h, \quad \tilde{u} = u/c, \quad \tilde{v} = v/c,$$
$$\tilde{\eta} = \eta/h, \quad \tilde{\psi} = \psi/(ch), \quad \tilde{t} = ct/h, \quad \tilde{p} = p/(\rho c^2).$$

where x, y, u and v are the axial and transverse co-ordinates and velocity components respectively, η is the transverse displacement of the wall, t time, p fluid pressure and ρ density. For convenience, all of the $\sim$ signs are omitted henceforth.

The boundary conditions governing the problems are

$$\eta = \epsilon\cos\alpha(x-t), \tag{2}$$

$$\partial\psi/\partial y = 0, \quad \partial\psi/\partial x = 0 \quad \text{at} \quad y = 1, \tag{3}$$

$$\partial\psi/\partial y = 0, \quad \partial\psi/\partial x = \alpha\epsilon\sin\alpha(x-t) \quad \text{at} \quad y = -1-\eta, \tag{4}$$

where ϵ is the amplitude ratio a/h, and α is the wave-number $2\pi h/\lambda$. Perturbation solutions in the parameter ϵ are assumed in the form

$$\psi = \psi_0+\epsilon\psi_1+\epsilon^2\psi_2+\ldots, \tag{5}$$

$$\left(\frac{\partial p}{\partial x}\right) = \left(\frac{\partial p}{\partial x}\right)_0+\epsilon\left(\frac{\partial p}{\partial x}\right)_1+\epsilon^2\left(\frac{\partial p}{\partial x}\right)_2+\ldots. \tag{6}$$

The term $(\partial p/\partial x)_0$ is the zeroth-order static pressure gradient. For an acid test of the theory we shall consider the case $(\partial p/\partial x)_0 = 0$. Then $\psi_0 = 0$, and we shall show later that the time average of the first-order term in pressure gradient, $(\partial p/\partial x)_1$, vanishes. Interestingly, the first-order terms of the time-averaged mean velocity, and mean mass flow, also vanish in this case; so that the mean pressure, velocity, and mass flow are all proportional to ϵ^2. The functions ψ_0, ψ_1, etc., defined in (5) can be shown to be

$$2\psi_1 = \Phi_1(y)\,e^{i\alpha(x-t)}+\Phi_1^*(y)\,e^{-i\alpha(x-t)}, \tag{7a}$$

$$2\psi_2 = \Phi_{20}(y)+\Phi_{22}(y)\,e^{2i\alpha(x-t)}+\Phi_{22}^*(y)\,e^{-2i\alpha(x-t)}. \tag{7b}$$

Substituting (6) and (7) into (1), (3) and (4) and equating the various powers of ϵ, one obtains, for the case of zero imposed pressure gradient, the following equations and boundary conditions for the first-order term:

$$\left[\frac{d^2}{dy^2}-\beta^2\right]\left[\frac{d^2}{dy^2}-\alpha^2\right]\Phi_1 = 0, \tag{8}$$

$$\Phi_1'(-1) = 0, \quad \Phi_1'(1) = 0, \tag{9a}$$

$$\Phi_1(-1) = -1, \quad \Phi_1(1) = 0. \tag{9b}$$

For the second-order terms one obtains

$$\Phi_{20}^{\mathrm{iv}} = -\tfrac{1}{2}i\alpha R_e(\Phi_1\Phi_1^{*\prime\prime\prime} - \Phi_1^*\Phi_1'')', \tag{10}$$

$$\left(\frac{d^2}{dy^2} - 4\alpha^2\right)\left[\frac{d^2}{dy^2} - (4\alpha^2 - 2i\alpha R_e)\right]\Phi_{22} = \tfrac{1}{2}i\alpha R_e(\Phi_1'\Phi_1'' - \Phi_1\Phi_1'''), \tag{11}$$

$$\Phi_{20}'(-1) - \tfrac{1}{2}[\Phi_1''(-1) + \Phi_1^{*\prime\prime}(-1)] = 0, \tag{12a}$$

$$\Phi_{20}'(1) = 0, \tag{12b}$$

$$\Phi_{22}'(-1) - \tfrac{1}{2}\Phi_1''(-1) = 0, \tag{13a}$$

$$\Phi_{22}(-1) - \tfrac{1}{4}\Phi_1'(-1) = 0, \tag{13b}$$

$$\Phi_{22}'(1) = \Phi_{22}(1) = 0. \tag{13c}$$

In the above, the primes denote differentiation with respect to y, the asterisks denote complex conjugate, and

$$\beta^2 = \alpha^2 - i\alpha R_e. \tag{14}$$

The solution to (8), subject to the boundary conditions (9), is

$$\Phi_1 = C_1\sinh(\beta y) + C_2\cosh(\beta y) + C_3\sinh(\alpha y) + C_4\cosh(\alpha y), \tag{15}$$

where C_1, C_2, C_3 and C_4 are integration constants.

On substituting (15) into (10) to (13), one can solve for Φ_{20} and Φ_{22}. The function Φ_{20}' can be posed in the form

$$\Phi_{20}' = M_1y^2 + M_2y + M_3 + F(y), \tag{16}$$

where M_1, M_2, M_3 are integration constants and $F(y)$ is a complicated function of y which was evaluated and is presented in full in Yin (1970). The constants M_1, M_2, M_3 are related through (12a), (12b). If one takes the time-average of the Navier–Stokes equation over one wave period to obtain a relation between the mean flow and mean pressure gradient, one obtains

$$\frac{\epsilon^2}{R_e}M_1 = \left(\overline{\frac{\partial p}{\partial x}}\right) = \epsilon^2\left(\overline{\frac{\partial p}{\partial x}}\right)_2. \tag{17}$$

Thus M_1 is proportional to the second-order mean pressure gradient and must be specified by the end conditions for each particular problem. With M_1 specified, the expression for the time-averaged mean axial velocity is

$$\bar{u} = \tfrac{1}{2}\epsilon^2\Phi_{20}' = \tfrac{1}{2}\epsilon^2\{F(y) - \tfrac{1}{2}[F(1) + F(-1)] + \tfrac{1}{2}\zeta + [-\tfrac{1}{2}\zeta + \tfrac{1}{2}[F(-1) - F(1)]]y - M_1(1 - y^2)\}, \tag{18}$$

where $\zeta = \tfrac{1}{2}[\Phi_1''(-1) + \Phi_1^{*\prime\prime}(-1)]$.

The mean flow per unit width is obtained by integrating (18):

$$\bar{q} = \int_{-1}^{1}\bar{u}\,dy = \tfrac{1}{2}\epsilon^2\left[\int_{-1}^{1}F(y)\,dy - [F(1) + F(-1)] + \zeta - \tfrac{4}{3}M_1\right]. \tag{19}$$

The mean volume flow expressed by (19) pertains to a two-dimensional channel of infinite width. In order to compare this quantity with the results from the

experimental work in which the width of the channel is finite, a correction factor to take into account the three-dimensional effect of the side walls is needed.

An approximate correction factor to account for the side-wall effect was obtained by the following considerations. The specific resistance of a rectangular cross-section uniform channel as a function of the width-to-height ratio† in a steady flow with a constant axial pressure gradient is well known, see, for instance, Rouse (1959) or Purday (1949). The result can be expressed as

$$\frac{dp}{dx} = -\frac{\mu U}{h^2} K\left(\frac{w}{h}\right), \tag{20}$$

where dp/dx is the pressure gradient, μ is the fluid viscosity, U is the mean velocity of flow, h is the channel half-height, w is the half-width, and K is the specific resistance factor which is a function of w/h, as shown in table 1. If the channel is

w/h	1	2	3	4	5	10	∞
K	28·6	17·5	15·3	14·2	13·7	12·8	12

TABLE 1. The specific resistance factor $K(w/h)$

two-dimensional, the corresponding resistance factor will be $K(\infty) = 12$ as $w/h \to \infty$. The mean flow per unit width of the channel is smaller by the factor $K(\infty)/K(w/h)$ because of the three-dimensional effect of the side walls. We assume that the same factor applies to the peristaltic flow, so that the mean flow per unit width is given by modifying $\bar{q}$ of (19) with the factor named above

$$Q = \bar{q}\frac{K(\infty)}{K(w/h)}. \tag{21}$$

The validity of this modification was checked experimentally, as will be described later.

To determine the velocity components u, v up to ϵ^2 the function Φ_{22} must be determined from (11) and (13):

$$\begin{aligned}\Phi_{22} = {} & F_1 \sinh\{y[2(\alpha^2+\beta^2)]^{\frac{1}{2}}\} + F_2 \cosh\{y[2(\alpha^2+\beta^2)]^{\frac{1}{2}}\} + \frac{D_1}{2(\alpha^2-\beta^2)}\sinh(2\alpha y) \\ & + \frac{D_2}{2(\alpha^2-\beta^2)}\cosh(2\alpha y) + J_1 \sinh(\beta y)\sinh(\alpha y) + J_2 \sinh(\beta y)\cosh(\alpha y) \\ & + J_3 \cosh(\beta y)\sinh(\alpha y) + J_4 \cosh(\beta y)\cosh(\alpha y).\end{aligned} \tag{22}$$

The constants $J_1, \ldots, J_4$ arise from the particular solution to (11) and are related to $C_1, \ldots, C_4$. The constants F_1, F_2, D_1, and D_2 arise from the complementary functions of (11) and can also be expressed, after considerable algebraic manipulation, in terms of $C_1, \ldots, C_4$.

† Henceforth, the expression 'width-to-height ratio' signifies channel half-width/channel mean half-height.

With these solutions the stream function ψ is determined up to ϵ^2 and the velocity components are

$$u = dx/dt = \tfrac{1}{2}\epsilon[\Phi_1'(y)\,e^{i\alpha(x-t)} + \Phi_1^{*\prime}(y)\,e^{-i\alpha(x-t)}] + \tfrac{1}{2}\epsilon^2[\Phi_{20}'(y) + \Phi_{22}'(y)\,e^{2i\alpha(x-t)} + \Phi_{22}^{*\prime}(y)\,e^{-2i\alpha(x-t)}],$$

$$v = dy/dt = -\tfrac{1}{2}\epsilon[i\alpha\Phi_1(y)\,e^{i\alpha(x-t)} - i\alpha\Phi_1^*(y)\,e^{-i\alpha(x-t)}] - \tfrac{1}{2}\epsilon^2[2i\alpha\Phi_{22}(y)\,e^{2i\alpha(x-t)} - 2i\alpha\Phi_{22}^*(y)\,e^{-2i\alpha(x-t)}]. \quad (23)$$

An integration of (23) yields the trajectory $x(t)$, $y(t)$ for any initial particle location. This integration was performed numerically by employing an extrapolation method devised by Bulirsch & Stoer (1966). An independent solution was also carried out using a standard Runge–Kutta–Dill numerical integration scheme. The two methods gave the same results to four significant figures, but the extrapolation method was said to be more accurate; therefore, all of the particle trajectories were obtained by using the extrapolation method. Calculation of one set of particle trajectories required between 6 and 10 min of computer time. Because of the considerable cost, only a limited number of cases were calculated. The results of the numerical calculations for the particle trajectories for a few cases and a comparison with the experimental results will be deferred to §4 pending the discussion of the experimental work to be presented in §3.

3. Experimental work

Apparatus

A rectangular cross-section channel with the top and side walls fixed and with a travelling wave imposed on the bottom wall was used. A sketch of the centre portion of the apparatus is shown in figure 2. A schematic diagram of the entire apparatus is shown in figure 3, and a photograph of the actual apparatus is shown in figure 4 (plate 1). The top, ends, and side walls, were made of lucite and the flexible bottom wall was a 0·079 cm thick neoprene sheet, slightly stretched and attached to the ends and sides of the channel. The overall channel length was 81·28 cm, its total height was 1·27 cm, and its width was 14·61 cm. These dimensions yielded a width-to-height ratio of 11·5 and a length-to-mean height ratio of 64.

The travelling sine wave was imposed on the flexible bottom wall by a series of moving plaster† blocks, B (figure 4), cast and polished to the desired amplitude and wavelength. The blocks were made so that aluminium plates with a series of teeth milled into their lower sides could be attached to the bottom of the blocks. These teeth were engaged by matching teeth of a timing belt C. The belt was driven by a speed reducer motor D controlled by a speed control unit to enable a range of wave speeds to be obtained. The weight of the fluid on top of the thin rubber membrane caused it to follow approximately the contour of the blocks. However, it was necessary to measure directly the vertical displacement of the membrane to obtain the actual wave amplitude.

The wave amplitude was measured by a probe connected to the core of a San-

† Toolstone, Dick Ellis Co., Los Angeles, California.

born linear differential transformer. As the blocks moved, the probe would follow the motion of the membrane and move the core accordingly. The transformer output was recorded on a strip chart recorder from which the actual wave amplitude could be calculated.

The longitudinal pressure gradient in the channel was controlled by two main reservoirs. The main reservoir at the upstream end had a stand pipe E which was fixed in height. The fluid level was maintained at this height by means of an external recirculating pump (not shown in figure 4) which pumped an excess

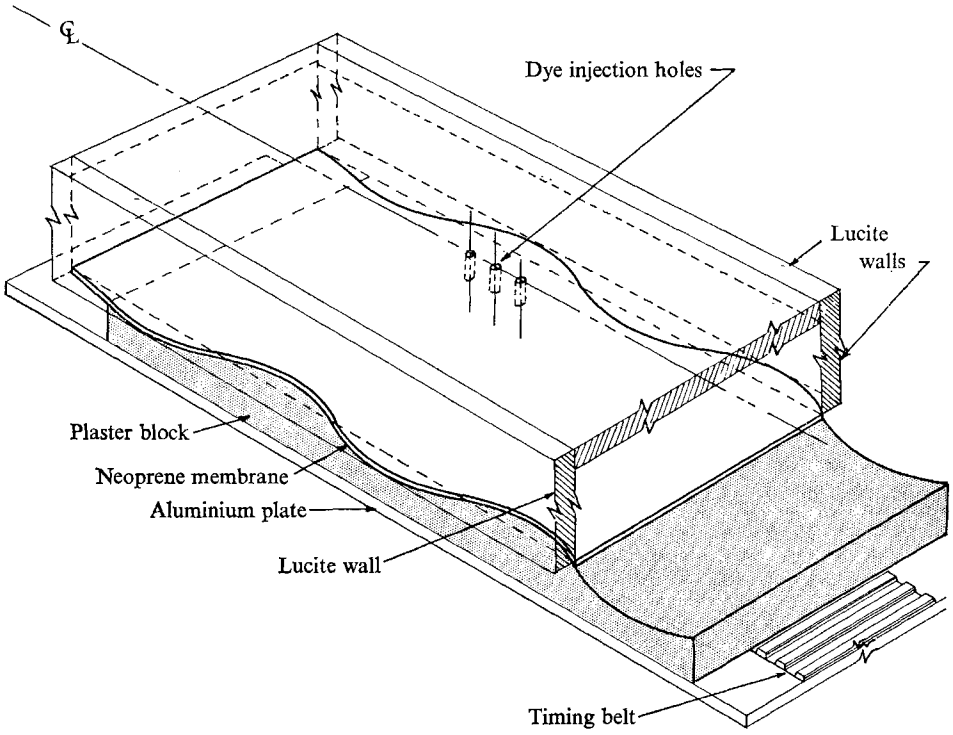

FIGURE 2. Sketch of the test section of the apparatus.

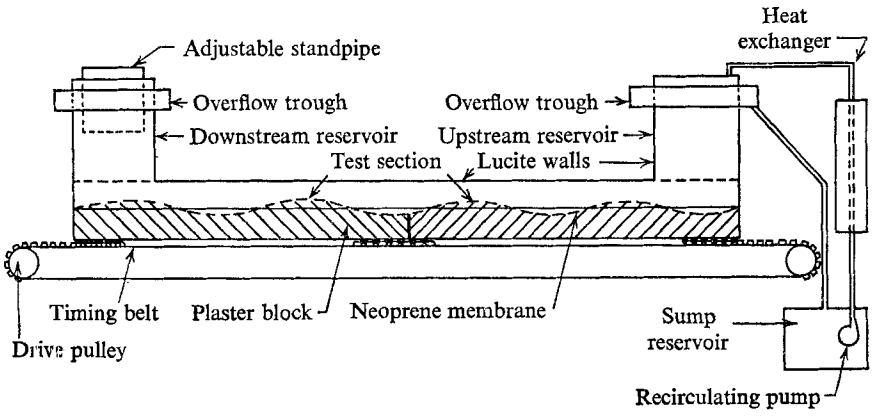

FIGURE 3. Schematic diagram of the apparatus.

of fluid into this reservoir. The overflow was then collected and recirculated by the external pump. The downstream reservoir had a height which could be varied by means of a movable standpipe F. The mean imposed pressure gradient was varied by raising or lowering this pipe relative to the upstream standpipe level. In both reservoirs the effects of surface tension were minimized by making the standpipes as large as possible with a very sharp top edge. The upstream standpipe was actually the reservoir wall itself. Recirculating fluid overflowed from inside the reservoir over the top edge and was collected by a trough surrounding the reservoir. The downstream standpipe was made slightly smaller than the reservoir and was circular. The standpipe was made movable by putting a lid on the reservoir with a circular hole slightly larger than the standpipe cut into the lid. The standpipe was inserted into this hole which had a rubber O-ring fitted into the rim. The O-ring sealed the gap while still allowing freedom of movement.

Fluid motion was studied by injecting dye at the test section A which was centred along the width and length of the channel. Any side-wall effects were expected to be minimal at the centre of the channel since the motion was symmetric between the side walls. In addition, results from classical fluid mechanics indicated that for steady flow at Reynolds numbers of order 10, the inlet length for a two-dimensional channel of the same dimensions as the present channel was of the order of the mean channel height. For small amplitude peristaltic waves, the end effects should not differ appreciably from those for steady flow conditions. Since the test section was located many times the mean channel height from the end, the end effects could be assumed to be negligible. Furthermore, by choosing the wavelength so that an integral number of waves was contained in the channel, the conditions equivalent to an infinite train of waves could be obtained. Therefore, for the apparatus used in this study, the fluid motion in the test section closely approximated the motion in an infinitely long two-dimensional channel.

The fluid was subjected to considerable viscous heating as it was continually being recirculated by the external pump. It was necessary to control the fluid temperature. This was accomplished by building a heat exchanger around the exit portion of the recirculating pump. The temperature in the water jacket was controlled by a recirculating cooler which then enabled the fluid in the channel to be kept at constant temperature. For all of the tests reported herein, the fluid was maintained at $25 \pm 0{\cdot}2$ °C.

The fluid used in all cases was Dow Corning 200 series silicone fluid which had a kinematic viscosity of 200 centistokes at 25 °C and a specific gravity of 0·97.

Procedure

Under a zero imposed pressure gradient condition, the total volume of fluid transported by the peristaltic motion of the walls as a function of the Reynolds number was measured at a given amplitude ratio (wave amplitude/channel mean half-height) and wave-number ($2\pi \cdot$ channel mean half-height/wavelength). Experiments were performed with two sets of waves having measured wave amplitudes of $0{\cdot}256 \pm 0{\cdot}006$ cm and $0{\cdot}174 \pm 0{\cdot}006$ cm respectively. In dimensionless quantities the amplitude ratios were $0{\cdot}41 \pm 0{\cdot}01$ and $0{\cdot}30 \pm 0{\cdot}01$ and the

wave-numbers were 0·385 and 0·353, respectively. By moving the blocks at different speeds, a range of Reynolds numbers from 0·5 to 2·5 was obtained.

By setting the downstream standpipe to the same height as the upstream reservoir, a condition of zero imposed pressure gradient could be maintained. At any given Reynolds number the steady-state volume of fluid transported in a given time interval was measured by collecting the overflow from the downstream standpipe. After suitable non-dimensionalization, the experimentally measured volume flow was then compared with the flow from theoretical prediction (see equations (21) and (19)). In each case the theoretical two-dimensional prediction of the flow was corrected by the scheme outlined previously to take into account the side-wall effect of the finite width-to-height ratio of the experimental apparatus.

In order to test experimentally the validity of applying the steady-state side-wall correction, two inserts of different size were placed into the channel to change the width-to-mean height ratio from 11·5 to 9·5 and 5·5. The inserts were made by glueing a piece of foam rubber to the bottom of a thin piece of lucite cut to the desired width, and running the length of the channel. The foam rubber was necessary to allow the flexible bottom wall to move vertically with the waves. The lucite and foam were covered with a polyethylene sheet to make the entire insert leakproof. The insert was held in place by the pressure exerted by the plaster blocks on the compressed foam rubber. The volume flow was then obtained as described previously and compared to the theoretically predicted flow with the correction factor for each width-to-height ratio included.

A small error in setting the zero imposed pressure gradient condition could produce a large error in the measured volume of fluid. The sensitivity of the flow to the accuracy of adjustment of the downstream standpipe was then tested by lowering and raising the pipe by a small amount from the assumed zero pressure gradient position. A lowering or raising of the pipe by 0·76 mm corresponded to imposing a pressure gradient of $\mp 0{\cdot}001$ cm H_2O per cm on the system. Volume flows corresponding to both positions of the standpipe were measured and compared with the value for the assumed zero-pressure-gradient position.

Since the theoretical solution is obtained by expansion in powers of ϵ (amplitude ratio), the accuracy of the theory is best when ϵ is small. However, experimentally, a lower limit of usable amplitude ratio exists because the highest accuracy with which the moving blocks could be made was about $\pm 0{\cdot}06$ mm. If ϵ is too small, the sine waves will be of poor quality and the accuracy of the amplitude of the successive waves will be low. A compromise satisfying the accuracy requirements of both the theory and experiment for the particle trajectory study was chosen at $\epsilon = 0{\cdot}2$, and was accomplished by modifying the channel height with a pair of new spacers. The trajectory data to be presented were obtained from a channel with a length-to-height ratio of 48, a width-to-height ratio of 8·0 and $\epsilon = 0{\cdot}20 \pm 0{\cdot}0055$ (S.D.).

Two methods were used to visualize the fluid motions. The first method consisted of injecting a line of tracer particles into the test section and photographing the subsequent distortion of the line. The tracer consisted of a suspension of finely powdered graphite in the same silicone fluid injected through a

no. 19-gauge hypodermic needle which was retracted gradually so as to leave a line. The distortion of the line was photographed with a motion picture camera. The second method consisted of injecting a small bubble of a neutrally buoyant immiscible fluid at various heights of the channel and recording the subsequent motion, which defined the particle trajectory. It was found that a mixture of two parts methanol to three parts milk gave a neutrally buoyant bubble which could be easily visualized in all portions of the channel. The particle path of a bubble starting at a given location in the channel was then obtained by measuring the positions of the bubble from motion picture recordings. These recordings were enlarged sixteen times by projecting onto a Vanguard Motion Analyzer,† which was equipped with movable cross-hairs connected to dials on which x and y positions could be read accurately to 0·001 in. The motion pictures were taken at eight frames per second and the position of the bubble was read from the analyzer at approximately $\frac{1}{2}$ sec intervals.

4. Results and discussion

(*a*) *Fluid transport*

The results of a series of tests employing three different width-to-height ratios and two different amplitude ratios showing the dimensionless volume flow as a function of the Reynolds number are illustrated in figure 5(*a*) and (*b*). The dotted line in each figure represents the value of the flow predicted by the two-dimensional theory and the solid line shows the two-dimensional volume flow corrected for the side wall effect. The open circles and triangles in each part of figure 5 represent the experimental data for amplitude ratios of 0·41 and 0·30 respectively. Parts (*a*) and (*b*) show results for width-to-height ratios of 11·5 and 5·5 respectively. The mean and standard deviation of the flow rate q/q_∞ are shown in figure 5(*c*) also for the width-to-height ratio of 9·5.

The filled circles and squares in figure 5(*a*) are data, taken with $\epsilon = 0{\cdot}41$, showing the sensitivity of the experiment to the accuracy of the setting of the downstream standpipe. The filled circles represent a setting that was 0·76 mm above the zero mean pressure gradient level, and the filled squares represent a setting 0·76 mm below the zero level. In this case, a pressure head of 0·76 mm corresponds to a pressure gradient of 0·001 cm H_2O per cm.

In figure 5(*c*) are plotted the ratios of the measured mass flow in channels of finite width divided by the corresponding theoretical values of the flow in channels of infinite width of the same values of mean height. The mean and standard deviation of the experimental data for Reynolds numbers in the range 0·5 to 2·5 are shown by the symbols. The solid line represents the theoretical approximate correction factor $K(\infty)/K(w/h)$ as proposed in (20). It is seen that at the smaller amplitude ratio ($\epsilon = 0{\cdot}30$) the approximation is justified.

The results shown in figures 5(*a*) and (*b*) demonstrate that, for $\epsilon = 0{\cdot}41$, there is about a 20% difference between the theoretical prediction (corrected for finite width-to-height ratio) and the experimental data. For $\epsilon = 0{\cdot}30$ the difference between theory and experiment is only about 3%. It is evident that, in

† Vanguard Instruments Corp., New York, N.Y.

the range tested, both theory and experiment indicate that the volume flow is relatively independent of the Reynolds number. The filled symbols in figure 5(*a*) show that the flow induced by a small amplitude wave is extremely sensitive to any mean imposed pressure gradients. Indeed, at the small mean pressure gradients purposely induced in the sensitivity tests ($\pm 0{\cdot}001$ cm H_2O/cm), the flow could be increased or decreased by about 15 %.

The closer agreement between theory and experiment at smaller values of ϵ is not surprising. Indeed it is gratifying that the agreement is good at ϵ as large as 0·30. The difference between theory and experiment may be attributed partly to experimental error, and partly to the basic limitations of the perturbation theory. The experimental error should be of the same magnitude for different values of ϵ, and is estimated to be a few percent. The theoretical analysis is carried out to the order of ϵ^2. Apparently for $\epsilon > 0{\cdot}30$ the higher-order terms may not be neglected.

The experimental results can also be compared with the theory of Shapiro (1967) who solved the problem of peristalsis on a channel with symmetric waves at zero Reynolds number and zero wave-number, $R_e = \alpha = 0$. In the limit $R_e = \alpha = \epsilon = 0$ the theories of Fung & Yih and Shapiro agree. Shapiro's theory can be modified quite easily for the case of one waving wall and corrected for side walls, the theoretical results on mean flow agree well with our experimental results at $\epsilon = 0{\cdot}30$, but are about 12 % larger than the experimental results when $\epsilon = 0{\cdot}41$. Thus although at $R_e = 0$ and $\alpha = 0$ Shapiro's solution is valid at all ϵ, at $R_e = 0{\cdot}5$ to 2 and $\alpha = 0{\cdot}57$ the discrepancy becomes significant at $\epsilon = 0{\cdot}41$. Recently Zien & Ostrach (1970) have carried out higher-order expansions in α (Shapiro's solution is the zero-order term in this scheme). A comparison of the higher-order theory with our experimental results should be done when such an analysis is extended to the one-waving-wall case.

On the other hand, part of these discrepancies could be due to the horizontal movement of the wall which was inherent in our experimental channel which employed a continuous inextensible belt as the moving wall. When the belt was forced to move up and down, no longitudinal restraint was imposed on the belt; hence a horizontal movement must be induced on the wall by the condition of inextensibility. For a sinusoidal wave $\eta = \epsilon \sin \alpha(x-t)$ the arc length s is

$$s \doteq (1+\tfrac{1}{4}\epsilon^2\alpha^2)\,x + \tfrac{1}{8}\epsilon^2\alpha[\sin 2\alpha(x-t) + \sin 2\alpha t] + O(\epsilon^4).$$

Hence, within ϵ^3:

$$x \doteq \frac{1}{1+\frac{1}{4}\epsilon^2\alpha^2}\,s - \frac{\epsilon^2\alpha}{8(1+\frac{1}{4}\epsilon^2\alpha^2)}\left\{\sin\left[2\alpha\left(\frac{s}{1+\frac{1}{4}\epsilon^2\alpha^2}-t\right)\right]+\sin 2\alpha t\right\}.$$

Since each particle on the belt is identified with a specific value of s, it is seen that the wall has a horizontal movement of amplitude approximately $\frac{1}{8}\epsilon^2\alpha$. For $\epsilon = 0{\cdot}3$ and 0·4 and $\alpha = 0{\cdot}57$, the amplitude of the horizontal movements are 0·0064 and 0·0114 respectively (in units of the half-width of the channel), i.e. 0·0214 and 0·0285 times the respective vertical movements. Although these are quite small, an exact evaluation of their effect is not available because all theories assumed purely vertical movement at the wall. One may note that most practical

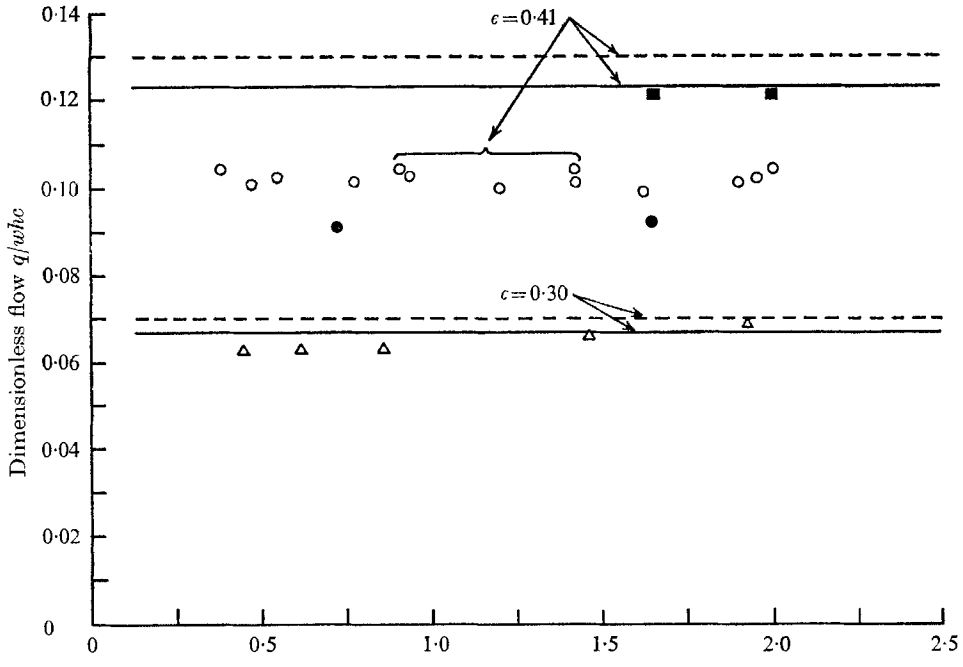

(*a*)

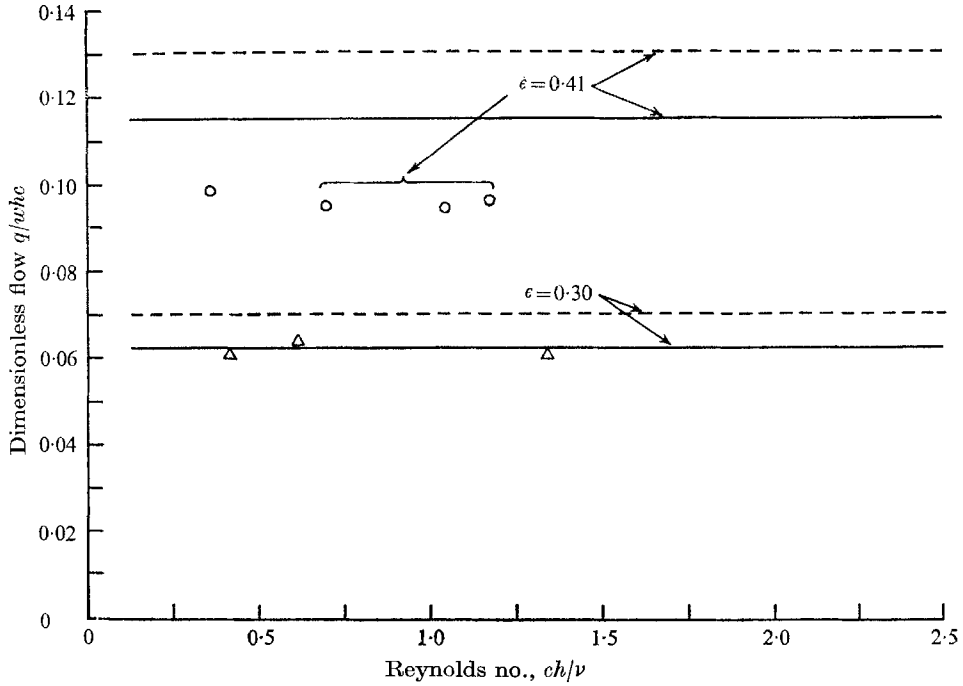

(*b*)

FIGURE 5(*a*), (*b*). For legend see facing page.

peristaltic pumps, including the animal ureters, have this type of wall, therefore, it may be desirable to work out the theoretical effects of the horizontal wall movement.

The results of the small imposed-pressure-gradient tests in figure 5(*a*) indicate the ineffectiveness of peristaltic pumping when the wave amplitude is not large. Practical peristaltic pumps generally occlude the vessel at its narrowest point, In normal human ureters each peristaltic wave sends only a single slug of fluid. which is followed by a long segment of tightly squeezed ureter with zero lumen.

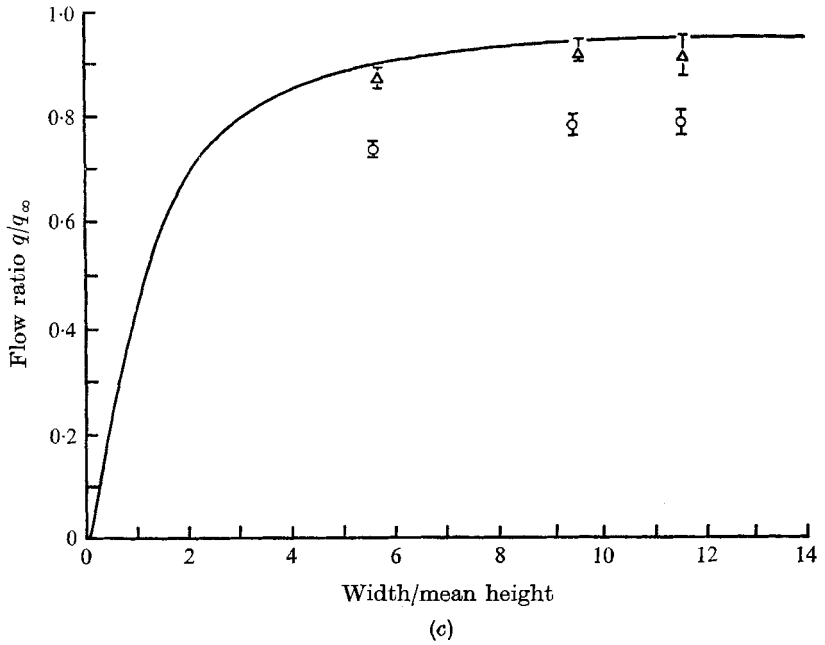

FIGURE 5. Comparison of theoretical and experimental results for the dimensionless flow *vs.* Reynolds number. Mean and standard deviation of data for R_e in the range 0·5 to 2·5 are shown. Width-to-height ratio: (*a*) 11·5; (*b*) 5·5. ϵ = amplitude ratio = amp/height. – – –, two-dimensional theory; ——, two-dimensional theory corrected for side walls; ●, downstream stand pipe raised 0·76 mm; ○, data for $\epsilon = 0{\cdot}41$; ■, downstream standpipe lowered 0·76 mm; △, data for $\epsilon = 0{\cdot}30$. (*c*) Comparison of results for the ratio of the flow in a finite width channel to the flow in a two-dimensional channel as a function of width-to-height ratio: ——, steady state theory for rectangular channel with no moving walls; ○, data for $\epsilon = 0{\cdot}41$; △, data for $\epsilon = 0{\cdot}30$.

(*b*) *Fluid motions*

Photographs of a fluid line taken at two-second intervals as the wave progressed under a condition of zero static pressure gradient for an amplitude ratio of 0·20 are shown in figure 6 (plate 2). Similar photographs taken under the condition of zero net flow are shown in figure 7 (plate 3). For the latter case the downstream reservoir was so raised that no fluid overflowed; consequently, a second-order (proportional to ϵ^2) static pressure gradient was imposed. In both figures the direction of wave travel is shown by the arrow. The successive frames are

arranged in columns. The period of motion in each figure is approximately 10 sec. The numbers indicate the beginning of successive wave periods. The first frame was taken with the blocks at rest, therefore the first few periods show the transient motion of the fluid due to the initial motion of the blocks.

It is difficult to assess quantitatively the motion of the fluid from pictures such as those in figures 6 and 7. However, the general behaviour of the fluid can be observed. Figure 6 shows that when no static pressure gradient was imposed on the system, all portions of the dyed line progressed downstream.

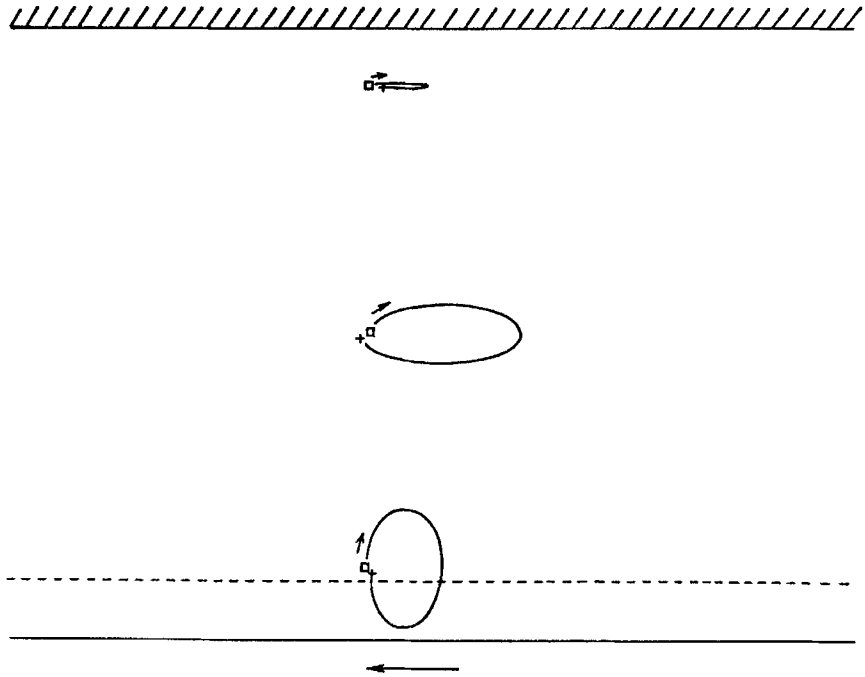

FIGURE 8. Theoretical trajectories for three particles. Zero volume flow condition with $\epsilon = 0{\cdot}2$, $R_e = 0{\cdot}6$, $\alpha = 0{\cdot}57$. □ initial location, $\frac{1}{4}$ wave ahead of the peak; +, position at end of one wave period; ——, mean position of wavy wall; – – – –, peak amplitude of wave; //////, position of fixed wall; ←, direction of wave travel.

Figure 7 is the more interesting case. It shows the distortion of the fluid line when there was no net flow in the system. It is seen that, even with the high degree of uniformity attained in the peak to peak amplitude of successive waves, there still are variations in the flow pattern. The net displacement of the dyed line is not monotonic in direction at corresponding times of successive periods, but shows some variation in magnitude and direction. In the long run, however, in regions near the fixed upper wall, the fluid moved in a direction opposite to the wave, while in the centre portion of the channel, the fluid progressed downstream but at a slower rate than that seen in figure 6. Near the moving wall it is difficult to assess the motion due to the similar colouring of the dye and the membrane. Further clarification of the fluid motion was obtained by examining the particle trajectories to be discussed below.

Consideration of the accuracy of both theory and experiment suggests that the best point for comparison of particle trajectories is at $\epsilon = 0{\cdot}2$. The comparison is given in figures 8 and 9. The results shown in figure 8 are the theoretically predicted trajectories for particles at three initial locations under a condition of zero net flow obtained with an amplitude ratio of 0·2. The corresponding experimental results are shown in figure 9. As mentioned previously, slight non-uniformities in successive waves caused variations in the fluid motion. The results shown in figure 9 are typical trajectories of particles which demonstrated a

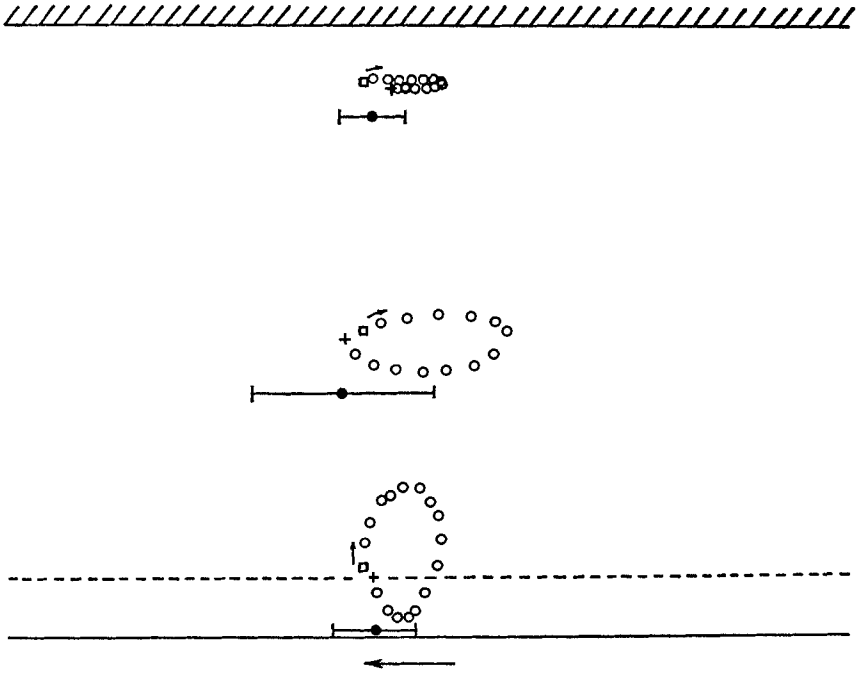

FIGURE 9. Experimental particle trajectories. Initial locations $\frac{1}{4}$ period ahead of wave peak. Zero volume flow condition with $\epsilon = 0{\cdot}2$, $R_e = 0{\cdot}6$, $\alpha = 0{\cdot}57$. The error bars denote the mean value and standard deviation of the net longitudinal displacement per wave period of the many trajectories examined.

net displacement per wave period close to the mean value obtained from studies of many trajectories. The error bar beneath each trajectory in figure 9 depicts the mean value and the standard deviation in the net longitudinal displacement per wave period. The open square indicates the initial position, the small arrow indicates increasing time, the cross mark indicates the position at the end of one wave period, and the large arrow indicates the direction of wave travel. It is seen that the theoretical and experimental trajectories are all qualitatively similar and that, on the average, the direction of net displacements per wave period is the same. The picture of the fluid motions obtained in this manner is also in qualitative agreement with the features shown in figure 7.

After each wave period of motion, a particle in general does not return to the same position relative to the wave. Therefore, one sees some vertical displace-

ment of a particle at the end of a wave period. It is easy to observe that the particle period is different from that of the wave period; but it is not generally realized that the difference can be very large. Some authors have contended that the particle period is the time for it to return to the initial height, at which point it repeats the same trajectory. But the last statement is in general untrue

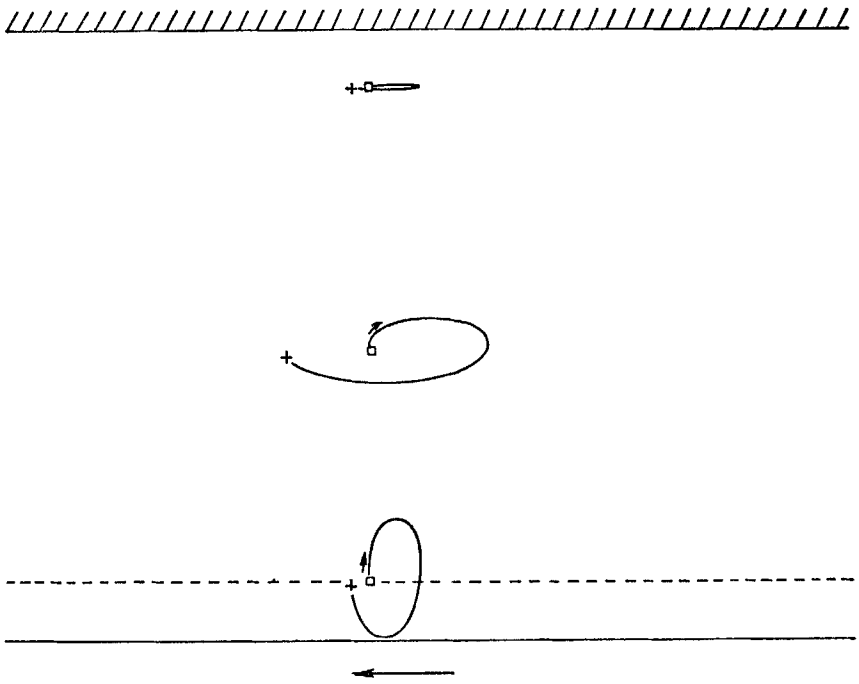

FIGURE 10. Theoretically predicted particle trajectories under zero mean imposed pressure gradient condition with $\epsilon = 0{\cdot}2$, $R_e = 0{\cdot}6$, $\alpha = 0{\cdot}57$. Initial locations $\frac{1}{4}$ period ahead of wave peak.

because at successive instants when the particle reaches the same height the horizontal displacements relative to the wave are different and the trajectory does not immediately repeat itself. Although eventually every particle path is periodic, the period can be grossly different from the successive time interval of returning to the same height. For this reason we choose to exhibit the particle path on the basis of wave period in figures 8 and 9.

For the sake of completeness, particle paths under a condition of zero imposed pressure gradient obtained theoretically for an amplitude ratio of 0·2 are shown in figure 10.

The qualitative agreement between theory and experiment as shown in figures 7, 8, and 9 lends confidence to the theoretical analysis. It should be pointed out that for the case of zero net flow, the results show that a particle near the middle of the channel experienced a net downstream displacement in the same direction as the wave motion. Particles near the walls showed net upstream displacements. The directions of displacements are the same as those found by Shapiro, Jaffrin & Weinberg (1969) for the symmetric two-waving-wall-channel case.

Finally, the difference in impressions about the fluid motion gained from the Eulerian and Lagrangian points of view can be compared. The Eulerian approach yields the time-averaged axial velocity under the condition of zero volume flow as shown in figure 11 (*a*). The Lagrangian approach yields the corresponding net horizontal displacements of fluid particles after each wave period. For sets of particles initially located along vertical lines positioned at $\frac{1}{4}$-wavelength

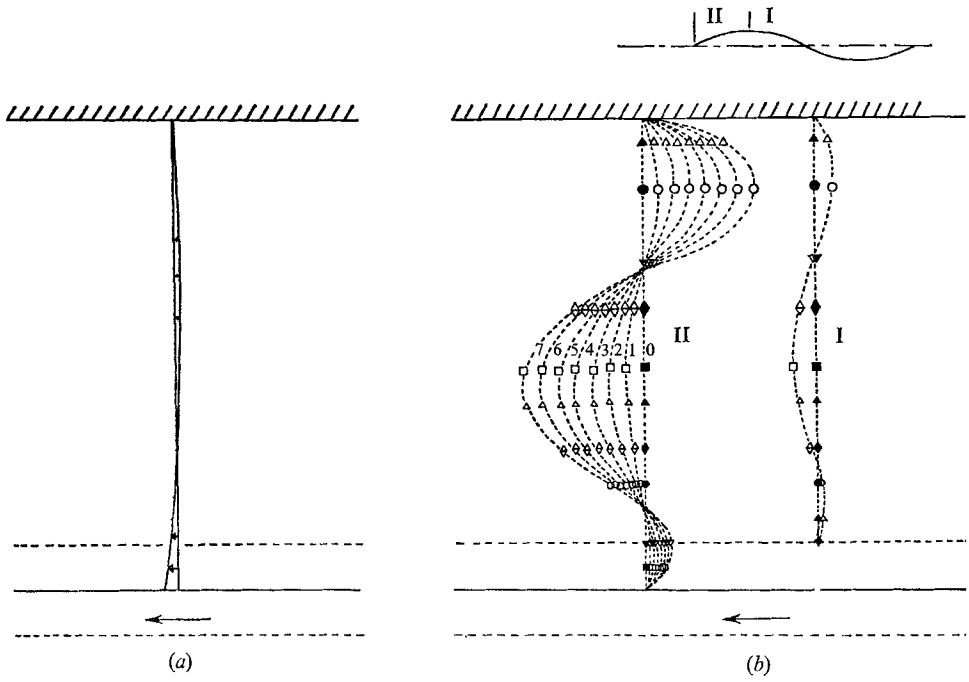

FIGURE 11. Comparison of time-averaged axial velocity (*a*) and net longitudinal displacement at the end of successive wave periods (*b*). Filled symbols indicate initial location. Open symbols denote position at the end of successive wave periods. Dotted lines connect particles of corresponding periods. Horizontal scale magnified by a factor of two. Inset shows a schematic picture of the initial location of each fluid line. Parameters: $\epsilon = 0{\cdot}2$, $R_e = 0{\cdot}6$, $\alpha = 0{\cdot}57$.

ahead of the peak and at the peak of the wave on the lower boundary (as shown schematically in the inset), the results are shown in figure 11 (*b*), in which the initial position of each particle is indicated by a filled symbol and the position at each successive wave period is indicated by the open symbol. The displacement profile per wave period is shown by the numbered dotted lines. The horizontal scale is magnified by a factor of two in order to show the details more clearly. The contrast between figures 11 (*a*) and (*b*) is remarkable. Near the centre of the channel, the mean axial velocity is negative, whereas the horizontal displacement (which may be divided by the wave period to give a kind of pseudo velocity) is positive. See the appendix for a more detailed discussion of this point.

A difference of opinion as to the definition of 'peristaltic reflux' exists in the literature, see the discussion of Fung & Yih's (1968) paper by Jaffrin & Shapiro

and the author's closure. Shapiro *et al.* prefer to define 'reflux' from a Lagrangian viewpoint saying that a flow exhibits 'reflux' whenever there is a negative net displacement of a particle trajectory. Fung & Yih define 'reflux' in the Eulerian sense by saying that a flow exhibits 'reflux' whenever there is a negative mean velocity in the flow field. These two definitions are different, and it is unfortunate that the same word was used for two different phenomena.

(c) *Conclusions*

The experimental work described in this paper demonstrated the following: (i) The time-averaged volume flow predicted by the two-dimensional theory (valid to second order in the amplitude ratio), corrected approximately for the three-dimensional finite width effect, is in close agreement with the experimental data for a value of amplitude ratio equal to 0·30. For a value of amplitude ratio equal to 0·41, there is about a 20 % difference between theory and experiment, due primarily to the limitations in the theory. (ii) The time-averaged volume flow is independent of the Reynolds number for the range $R_e < 2{\cdot}5$. (iii) Peristaltic pumping with small amplitude waves is an ineffective method for transporting fluid, because a very small imposed pressure gradient can overwhelm the effect of the peristalsis. (iv) Particle trajectories for the case of zero volume flow were found to agree qualitatively with the theoretical predictions for a value of the amplitude ratio equal to 0·2.

This work was supported by USPHS Grant HE 12494-01 by the National Institute of Health, Grant GK-10552 by the National Science Foundation, and Grant 1186-67 by U.S. Air Force Office of Scientific Research.

Appendix. Stroboscopic velocity of fluid particles

The trajectories of fluid particles in a channel subjected to peristaltic pumping as shown in figures 8–11, are rather complex and have periods grossly different from that of the wall. A simpler view of the fluid motion is to look at the particles stroboscopically. We label each particle initially with co-ordinates a, b, c; then examine its trajectory $x_i = x_i(a, b, c, t)$ periodically at an interval equal to the wave period, T. At the nth period $t = nT$ the particle is located at

$$(x_i)_n \quad (i = 1, 2, 3).$$

We define an apparent velocity

$$(V_i)_n = \frac{(x_i)_{n+1} - (x_i)_n}{T} \quad (i = 1, 2, 3), \tag{A 1}$$

which is what the particle would reveal to an observer who looks at the flow with a stroboscopic light of period T. V_i is not the velocity of motion of the particle in the ordinary sense. We shall call V_i the *stroboscopic velocity* of the particle.

Figure 11 (*b*) shows the stroboscopic displacements $(x_i)_n$. The contrast between figures 11 (*a*) and (*b*) shows that V_i has little resemblance with the mean velocity $\bar{u}_i$, which can be defined equivalently either by averaging over time at a fixed

location or by averaging over x at fixed y, z, and t. An explicit examination of this difference is given below in a particular case.

Consider the peristaltic pumping of a two-dimensional channel of constant pair width with a pair of symmetrically posed sinusoidal progressive waves moving down the opposite walls as is discussed in the paper of Fung & Yih (1968). Let us consider the motion of the particles on the centre line, $y = 0$. In the case of 'free pumping' (in an originally stationary fluid) these particles move in the axial direction with the velocity

$$u(x,0,t) = \tfrac{1}{2}\epsilon[\Phi_1'(0)\,e^{i\alpha(x-t)} + \Phi_1^{*\prime}(0)\,e^{-i\alpha(x-t)}] + \tfrac{1}{2}\epsilon^2[\Phi_{20}'(0) + \Phi_{22}'(0)\,e^{2i\alpha(x-t)} + \Phi_{22}^{*\prime}(0)\,e^{-2i\alpha(x-t)}] + O(\epsilon^3). \quad (A\,2)$$

The functions $\Phi_1(y)$, $\Phi_{20}(y)$, etc., are given in the reference named above. The mean velocity is

$$\overline{u}(0) = \tfrac{1}{2}\epsilon^2\Phi_{20}'(0). \quad (A\,3)$$

On the other hand, for a particle located at $x = a$, $y = 0$, when $t = 0$, the trajectory $x(a,0,t)$ must satisfy the equation

$$dx(a,0,t)/dt = u[x(a,0,t),t]. \quad (A\,4)$$

Substituting $u(x,0,t)$ from the right-hand side of (A 2), integrating with respect to t, and noting the initial position $x = a$, one obtains

$$x(a,0,t) = a + \epsilon\,\mathrm{Re}\left\{\int_0^t \Phi_1'(0)\,e^{i\alpha[x(a,0,t)-t]}\,dt\right\} + \epsilon^2\left[\Phi_{20}'(0)\,\tfrac{1}{2}t + \mathrm{Re}\left\{\int_0^t \Phi_{22}'(0)\,e^{2i\alpha[x(a,0,t)-t]}\,dt\right\}\right]. \quad (A\,5)$$

A first approximation is obtained by substituting a for x in the integrals in (A 5). A second substitution yields the second approximation

$$x(a,0,t) = a + \epsilon\,\mathrm{Re}\left\{\Phi_1'(0)\frac{e^{i\alpha a}(1-e^{-i\alpha t})}{i\alpha}\right\} + \epsilon^2\left\{\tfrac{1}{2}\Phi_{20}'(0)\,t + \mathrm{Re}\left[\Phi_{22}'(0)\frac{e^{2i\alpha a}(1-e^{-2i\alpha t})}{2i\alpha}\right]\right\} + \epsilon^2\,\mathrm{Re}\left\{[\Phi_1'(0)]^2 e^{2i\alpha a}\left[\frac{1-e^{-i\alpha t}}{i\alpha} - \frac{1-e^{-2i\alpha t}}{2i\alpha}\right] - |\Phi_1'(0)|^2\left[\frac{1-e^{-i\alpha t}}{i\alpha} - t\right]\right\} + O(\epsilon^3). \quad (A\,6)$$

Hence we obtain the stroboscopic velocity at $t = 2n\pi/\alpha$:

$$\begin{aligned} V(a,0,t) &= (\alpha/2\pi)\{x[a,0,(n+1)\,2\pi/\alpha] - x[a,0,n2\pi/\alpha]\} \\ &= \tfrac{1}{2}\epsilon^2\{\Phi_{20}'(0) + |\Phi_1'(0)|^2\} \\ &= \overline{u}(0) + \epsilon^2|\Phi_1'(0)|^2. \end{aligned} \quad (A\,7)$$

In the case of zero net volume flow, $\overline{u}(0)$ is negative, but $V(a,0,t)$ is positive because of the last term.

This analysis shows clearly the mechanism with which the fluid particle moves against the stream. The large (first order in ϵ) sinusoidal oscillation makes no net contribution to the mean motion at any location, but every fluid particle is carried by this first-order term to move in a nearly elliptical trajectory with a major axis proportional to ϵ, which is much smaller than the wavelength $2\pi/\alpha$. The particle on this trajectory is displaced out of phase with respect to the wave motion, and no longer sees the velocity field as harmonic. In this way a non-vanishing second-order stroboscopic velocity is obtained.

REFERENCES

BARTON, C. & RAYNOR, S. 1968 Peristaltic flow in tubes. *Bull. Math. Biophys.* **30**, 663–680.

BURLIRSCH, R. & STOER, J. 1966 Numerical treatment of ordinary differential equations by extrapolation methods. *Num. Math.* **8**, 1–13.

BURNS, J. C. & PARKES, T. 1967 Peristaltic motion. *J. Fluid Mech.* **29**, 731–743.

FUNG, T. C. & YIH, C. S. 1968 Peristaltic transport. *Trans. ASME, J. Appl Mech.* **35**, 669–675. Discussion by M. Jaffrin and A. Shapiro and author's closure, **36**, 379–381.

HANIN, M. 1968 The flow through a channel due to transversely oscillating walls. *Israel J. Tech.* **6**, 67–71.

LATHAM, T. W. 1966 Fluid motions in a peristaltic pump. SM thesis, Mechanical Engineering Department, Massachusetts Institute of Technology.

PURDAY, H. F. P. 1949 *An Introduction to the Mechanics of Viscous Flow.* Dover.

ROUSE, H. 1959 *Advanced Mechanics of Fluids.* John Wiley.

SHAPIRO, A. H. 1967 Pumping and retrograde diffusion in peristaltic waves. *Proc. Workshop in Ureteral Reflux in Children, Nat. Acad. Sci., Nat. Res. Council*, pp. 109–126.

SHAPIRO, A. H., JAFFRIN, M. Y. & WEINBERG, S. L. 1969 Peristaltic pumping with long wavelengths at low Reynolds numbers. *J. Fluid Mech.* **37**, 799–825.

YIN, F. 1970 Theoretical and experimental investigations of peristaltic motion. Ph.D dissertation, Dept. of Aerospace and Mechanical Engineering Sciences, University of California, San Diego.

YIN, F. & FUNG, Y. C. 1969 Peristaltic waves in circular cylindrical tubes. *Trans. ASME, J. Appl. Mech.* **36**, 579–587.

ZIEN, T. F. & OSTRACH, S. 1970 A long wave approximation to peristaltic motion. *J. Biomechanics*, **3**, 63–75.

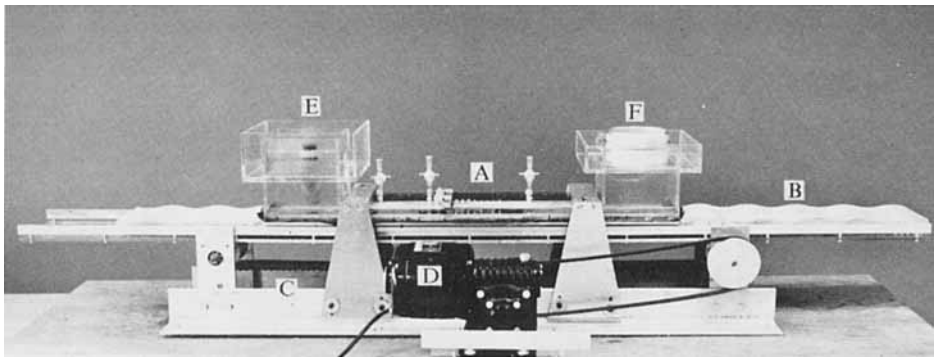

FIGURE 4. Photograph of the apparatus. A, Test section; B, Plaster blocks; C, Timing belt; D, Variable speed motor; E, Upstream reservoir; F, Adjustable standpipe in downstream reservoir.

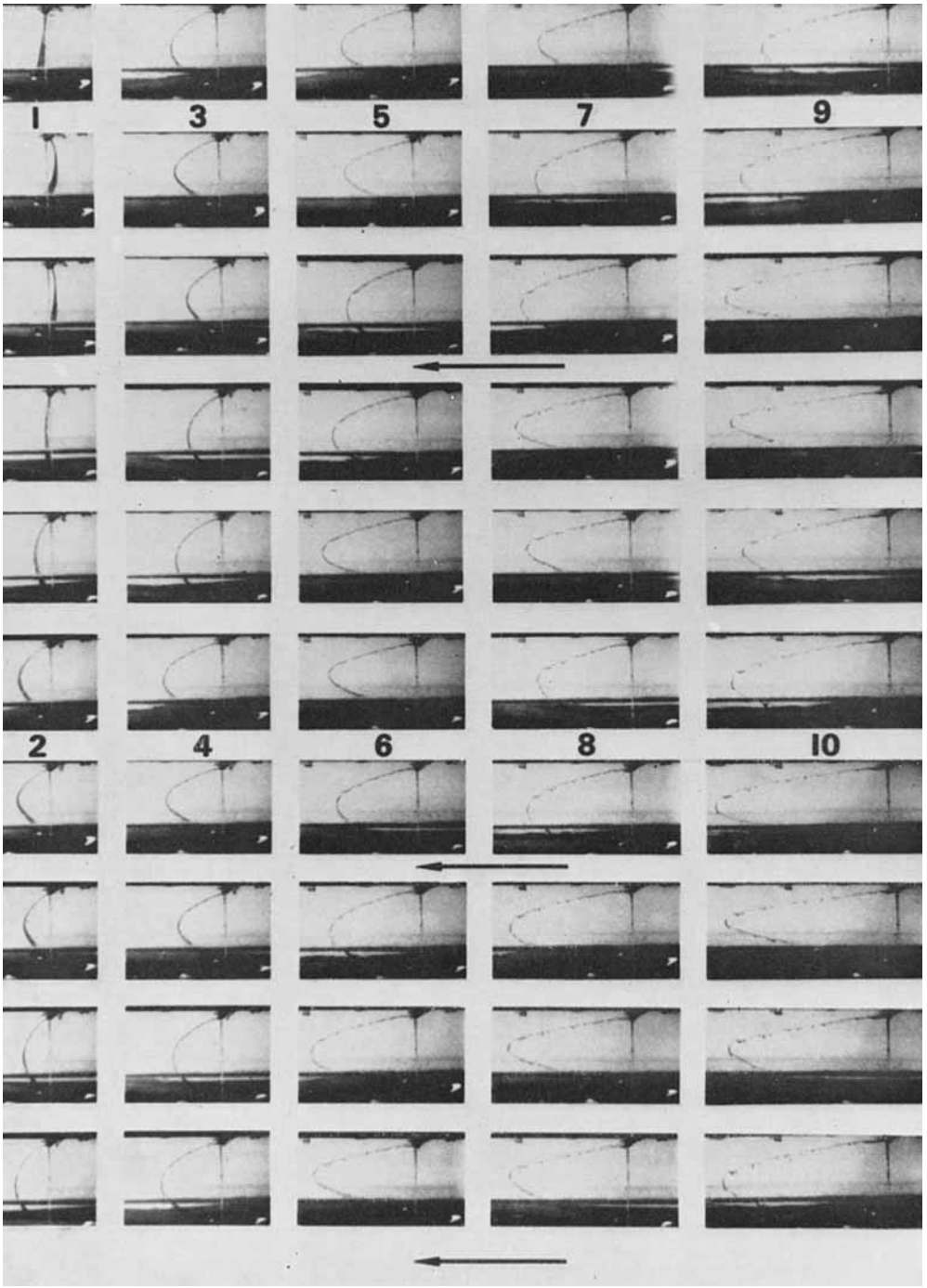

FIGURE 6. Distortion of a fluid line under zero mean imposed pressure gradient conditions. Photographs at two second intervals starting from rest. Waves moving from right to left. Numbers below photos denote the approximate beginning of successive wave periods. Parameters: $R_e = 0{\cdot}6$, $\alpha = 0{\cdot}57$, $\epsilon = 0{\cdot}2$.

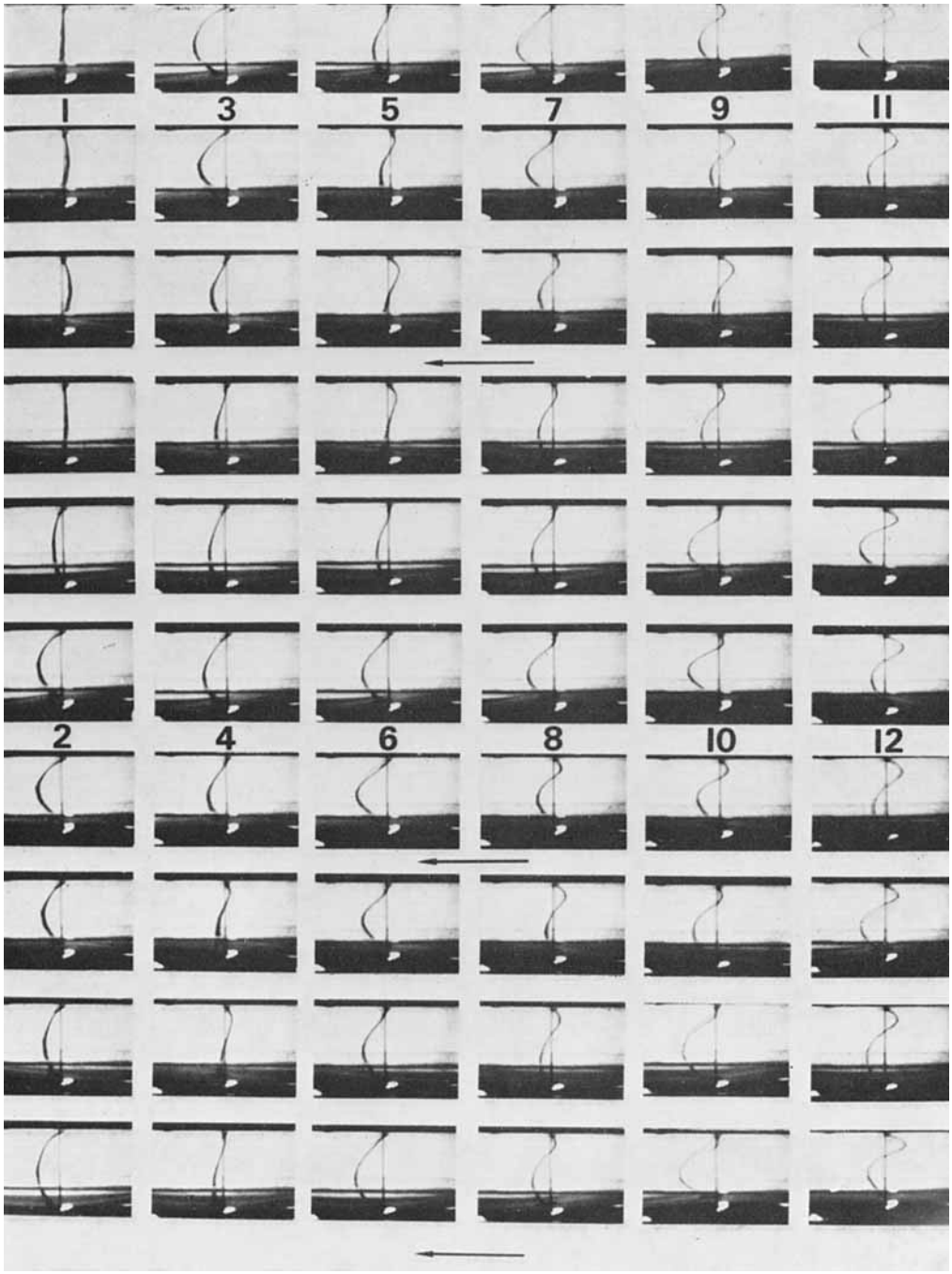

FIGURE 7. Distortion of a fluid line under zero volume flow conditions. Photographs at two second intervals starting from rest. Waves moving from right to left. Numbers below photos denote the approximate beginning of successive wave periods. Parameters: $R_e = 0{\cdot}6, \alpha = 0{\cdot}57, \epsilon = 0{\cdot}2$.